Prediction for unintegrated parton distributions

Jianhong Ruan and **Wei Zhu**

Department of Physics, East China Normal University, Shanghai 200062, P.R. China

Abstract

Unintegrated parton distributions in the proton and nucleus are predicted by a modified DGLAP equation incorporating the shadowing corrections, which include exact energy-momentum conservation in each splitting and fusion vertices. We find that the nuclear shadowing effects are obvious, although they are far from the saturation limit. On the other hand, we point out that the suppression of the unintegrated gluon distribution toward lower k_t^2 may arise from the valence-like input rather than the saturation effects.

1 Introduction

Conventional parton distribution functions (PDFs) are the basic quantities describing the inclusive cross sections of hard processes within the QCD improved parton model. These distributions are integrated over the transverse momentum k_t of an observed parton to the virtuality μ^2 of the probe. Describing the exclusive processes, where the transverse momentum of the produced hadron can be observed, requires the introduction of more complicated quantities, the so-called (two-scale) unintegrated parton distribution functions (UPDFs), which generally depend on two hard scales k_t and μ. Recently, theoretical and phenomenological studies of UPDFs have been actively pursued since they exactly correspond to the quantity that enters the Feynman diagrams and relate to many exclusive or semiexclusive processes; For a review, see Ref. [1].

An existing evolution equation for the two-scale unintegrated gluon distribution is the CCFM equation [2], in which the emission of gluons during the initial cascade is only allowed in an angular-ordered region. The corresponding quark distributions are indirectly derived by the convolution of the gluon density with the off-shell matrix element for boson gluon fusion. The solution of the CCFM equation is much more complicated and has only proven to be practical with Monte Carlo generators up to now. Moreover, the interactions among initial partons are neglected in the derivation of the CCFM equation. Obviously, this assumption is invalid at the small-x and low-k_t regions, where the parton wave functions begin overlap spatially. Therefore, the corrections of the initial gluon fusion to the QCD evolution equation at small-x should be considered. One can imagine that gluon fusion suppresses or shadows the growth of parton densities and leads the parton distribution gradually approaching a possible limit form at $k_t < Q_s(x)$, where the

2

gluon fusion balances with the gluon splitting. This stable form is called the saturation [3]. The value of Q_s^2 is the saturation scale. The behavior of UPDFs near the saturation scale is important for testing various nonlinear QCD evolution dynamics. Although some recent works [4] used an absorptive boundary condition on the CCFM equation to mimic the saturation effect, it is quite cumbersome to introduce the gluon recombination kernels in the CCFM equation.

Instead of the CCFM equation, Kimber, Martin and Ryskin [5] proposed that the two-scale UPDFs can be derived from the single-scale unintegrated distribution, and its dependence on the second scale μ is introduced by using the Sudakov factor. The single-scale unintegrated distributions can be obtained by the following different ways: (i) the KMS scheme [6]: the BFKL equation embodying leading log k_t^2 (DGLAP) corrections; or (ii) the KMR scheme [5]: the DGLAP equation embodying leading log $1/x$ (BFKL) corrections. Compared with the CCFM equation, the modifications of the gluon fusion to the BFKL and DGLAP equations are easily made.

A modification of the gluon fusion to the BFKL equation is the BK equation [7]. Both the BFKL and BK equations include only the leading-order $(1/x)$ (LLx) contributions, and they work at the small-x range. The beyond LLx modifications should be included for the predictions in the full-x range. However, it is difficult to treat the subleading logarithmic corrections in the BFKL and BK dynamics, except for making a roughly approximation [8].

The correction of the gluon recombination to the DGLAP equation was first proposed by Gribov-Levin-Ryskin and Muller-Qiu in the GLR-MQ equation [9,10]. In this equation, the double leading logarithmic approximation ($DLLA$) was taken, where the nonlinear

shadowing terms only kept the $1/x$ power contributions. Obviously, the beyond LLx corrections to the GLR-MQ kernel are necessary. We have generalized the GLR-MQ equation in a modified DGLAP (MD-DGLAP) equation, in which the evolution kernels were derived in the full-x range at the $LL(Q^2)$ approximation [11]. On the other hand, the corrections of the BFKL effect due to the random distribution of transverse momenta at the small-x range are small in the KMR scheme [5], and we neglect them in this work. Thus, we may obtain the two-scale UPDFs based on the DGLAP dynamics including the shadowing effect. This is one of the reasons why we try to evolve the two-scale UPDFs by using the MD-DGLAP equation. Besides, the linear DGLAP evolution and nonlinear recombination corrections in the MD-DGLAP equation were derived by using the cutting rules based on the time-ordered perturbation theory (TOPT), where the contributions from the real and virtual diagrams to the MD-DGLAP equation were naturally separated. Thus, we can easily calculate the virtual contributions with the Sudakov form factor in the KMR scheme.

At a first step, we compute the MD-DGLAP equation with the data from the HERA to obtain a set of integrated parton distributions in Sec. 2. The numerical solutions of the evolution equation depend sensitively on the input parton distributions at some low scale μ_0. In this work, we use the GRV model [12], in which the parton distributions are QCD radiatively generated from the valence-like input distributions at an optimally determined scale $\mu_0 < 1 \ GeV$. Therefore, the behavior of the parton densities at $k_t^2 > \mu_0^2$ is a purely perturbative phenomenon. This radiative approach is especially important for the investigations concerning asymmetrical behaviors of UPDFs at small x and low k_t^2. Therefore, in this work we use the GRV-type input distributions to evolve the MD-

DGLAP equation.

In Sec. 3 we use the above-mentioned integrated parton distributions to predict the UPDFs in the KMR scheme. We discussed the comprehensive effects of the nonlinear terms in the evolution equation. To emphasize the shadowing effect, we calculate the two-scale UPDFs in the nuclear target. An interesting result is that we find that the unintegrated gluon distribution is dropping toward low k_t and it arises from the valence-like input rather than the nonlinear saturation effects. As we know that several UPDFs with the saturation model have been used to explain the inclusive hadronic production at the RHIC and further to predict the LHC physics, our result provides an alternative model without the nonlinear saturation mechanism. We will discuss this result in the last section.

2 Modified DGLAP equation

We determine a set of integrated parton distributions with the QCD evolution equation by fitting the HERA measurements of the proton structure function F_2. We know that the DGLAP equation produces a rapid growth of gluon density at small x. The gluons therefore must begin to spatially overlap and recombine. The corrections of parton recombination to the DGLAP equation in Ref. [11] were considered by summing up all possible twist-four cut diagrams at the $LLA(Q^2)$. In the derivation of the equation, the TOPT was used to pick up the contributions of the leading recombination diagrams. As a consequence, the corrections of the gluon recombination to the evolution of PDFs near scale Q^2 are described by the following modified DGLAP equation:

$$
Q^2 \frac{dxv(x, Q^2)}{dQ^2}
$$
$$
= \frac{\alpha_s(Q^2)}{2\pi} \int_x^1 \frac{dy}{y} P_{qq}(z) xv(y, Q^2)
$$
$$
- \frac{\alpha_s(Q^2)}{2\pi} xv(x, Q^2) \int_0^1 dz P_{qq}(z), \tag{1}
$$

for valence quark distribution, where $z = x/y$,

$$
Q^2 \frac{dxs(x, Q^2)}{dQ^2}
$$
$$
= \frac{\alpha_s(Q^2)}{2\pi} \int_x^1 \frac{dy}{y} P_{qq}(z) xs(y, Q^2)
$$
$$
+ \frac{\alpha_s(Q^2)}{2\pi} \int_x^1 \frac{dy}{y} P_{qg}(z) xg(y, Q^2)
$$
$$
- \frac{\alpha_s(Q^2)}{2\pi} xs(x, Q^2) \int_0^1 dz P_{qq}(z)
$$
$$
- \frac{\alpha_s^2(Q^2) K}{Q^2} \int_x^{1/2} \frac{dy}{y} x P_{gg \to q}(z) [yg(y, Q^2)]^2
$$

$$+\frac{\alpha_s^2(Q^2)K}{Q^2}\int_{x/2}^x \frac{dy}{y} x P_{gg\to q}(z)[yg(y,Q^2)]^2, \tag{2}$$

for sea quark distribution, and

$$Q^2\frac{dxg(x,Q^2)}{dQ^2}$$

$$=\frac{\alpha_s(Q^2)}{2\pi}\int_x^1 \frac{dy}{y} P_{gq}(z) x s(y,Q^2)$$

$$+\frac{\alpha_s(Q^2)}{2\pi}\int_x^1 \frac{dy}{y} P_{gg}(z) x g(y,Q^2)$$

$$-\frac{1}{2}2n_f\frac{\alpha_s(Q^2)}{2\pi}xg(x,Q^2)\int_0^1 dz P_{qg}(z)$$

$$-\frac{1}{2}\frac{\alpha_s(Q^2)}{2\pi}xg(x,Q^2)\int_0^1 dz P_{gg}(z)$$

$$-\frac{\alpha_s^2(Q^2)K}{Q^2}\int_x^{1/2}\frac{dy}{y} x P_{gg\to g}(z)[yg(y,Q^2)]^2$$

$$+\frac{\alpha_s^2(Q^2)K}{Q^2}\int_{x/2}^x \frac{dy}{y} x P_{gg\to g}(z)[yg(y,Q^2)]^2, \tag{3}$$

for gluon distribution, where the unregularized DGLAP splitting kernels are

$$P_{gg}(z) = 2C_2(G)\left[z(1-z) + \frac{1-z}{z} + \frac{z}{1-z}\right], \tag{4}$$

$$P_{gq}(z) = C_2(R)\frac{1+(1-z)^2}{z}, \tag{5}$$

$$P_{qq}(z) = C_2(R)\frac{1+z^2}{1-z}, \tag{6}$$

$$P_{qg}(z) = \frac{1}{2}[z^2 + (1-z)^2], \tag{7}$$

$$C_2(G) = N = 3, \quad C_2(R) = \frac{N^2-1}{2N} = \frac{4}{3}, \tag{8}$$

and the recombination functions are

$$P_{gg \to g}(z) = \frac{9}{64} \frac{1}{x}(2 - z)(72 - 48z + 140z^2 - 116z^3 + 29z^4), \tag{9}$$

$$P_{gg \to q}(z) = \frac{1}{48} \frac{1}{x} z(2 - z)^2(18 - 21z + 14z^2). \tag{10}$$

The parameter K in Eqs. (1)-3) depends on the definition of double parton distribution and the geometric distributions of partons inside the target. For simplicity, we regard K as a free parameter. The factor $1/2$ in the virtual terms of Eq. (3) due to the symmetry of the Feynman diagrams is important for the cancellation of the collinear singularities [11].

In the derivation of the above-mentioned MD-DGLAP equation, the TOPT cutting rules were used [11]. The contributions of the DGLAP equation and the recombination corrections are presented in the MD-DGLAP equation in a unified methodology. The contributions from the real and virtual diagrams are completely separated although they share a common evolution kernel. Thus, we can completely extract the contributions from the virtual processes using the Sudakov from factor in Sec. 3. This form of the linear parts in Eqs. (1)-(3) was first derived by Collins and Qiu using the technique of cut vertices in Ref. [13], but they can be more simply confirmed with the TOPT cutting rules [11].

The nonlinear parts of Eqs. (1)-(3) are the contributions from $2 \to 2$ and $1 \to 3$ recombination processes. The equation keeps the momentum conservation. Particularly, the positive nonlinear terms contribute the antishadowing effect, while the negative nonlinear terms lead to the shadowing correction. The coexistence of shadowing and antishadowing

in the QCD evolution equation is a general requirement of the local momentum conservation. The GLR-MQ equation does not consider the contributions from the virtual diagrams of the recombination processes. Fortunately, we have indicated that the contributions from the virtual diagrams corresponding to $2 \rightarrow 2$ and $1 \rightarrow 3$ recombination processes are canceled [11]. Thus, we do not need to compute the virtual diagrams of the nonlinear recombination processes in the Sudakov form factor, provided the equation includes the contributions from both the shadowing and antishadowing effects.

We emphasize that the combining distribution of two gluons is assumed to be $g^{(2)}(y, Q^2) = g^2(y, Q^2)$ either in the MD-DGLAP equation or in the GLR-MQ equation. This is the simplest model. One of us (W.Z) has discussed the recombination of gluons with different values of x in the nonlinear evolution equation and finds that this modification unreasonably enhances the shadowing effect in the GLR-MQ equation, while it does not change the predictions of the MD-DGLAP equation, since the momentum conservation plays an important role in this result [14].

Since the equations (1)-(3) were derived at the leading logarithmic (Q^2) approximation and they contain the terms beyond the leading logarithmic $1/x$ approximation, the modified DGLAP equation is valid in the full-x range if we neglect the BFKL corrections at the very small-x region.

In this work we use the initial valence quark and gluon densities in the GRV98LO set [12], that is

$$xu_v(x, \mu_0^2) = 1.239x^{0.48}(1 - x)^{2.72}(1 - 1.8\sqrt{x} + 9.5x),$$

$$xd_v(x, \mu_0^2) = 0.614(1 - x)^{0.9} xu(x, \mu_0^2),$$

and

$$xg(x, \mu_0^2) = 17.47x^{1.6}(1 - x)^{3.8}. \tag{11}$$

In the meantime, we let the parameters in the sea quark distribution to fit the HERA data [15] using the MD-DGLAP evolution equation. As a consequence, this input sea quark distribution in the GRV98LO,

$$xs(x, \mu_0^2) = 2x[\overline{u} + \overline{d}]$$

$$= 1.52x^{0.15}(1 - 3.6x^{0.5} + 7.8x)(1 - x)^{9.1}, \tag{12}$$

is changed to

$$xs(x, \mu_0^2) = 2x[\overline{u} + \overline{d}]$$

$$= 0.9x^{0.01}(1 - 3.6x^{0.5} + 7.8x)(1 - x)^{8.0}, \tag{13}$$

and the starting scale of the evolution is modified from $\mu_0^2 = 0.26 GeV^2$ to $\mu_0^2 = 0.34 GeV^2$.

To illustrate the difference between the two input distributions, we plot in Fig. 1 our modified input sea quark distribution $xs = 2x[\overline{u} + \overline{d}]$ of Eq. (13) (solid curve) and that of the GRV98LO of Eq. (12) (dashed curve). Our distribution is soften than the GRV98LO set for compensating the shadowing effect in the evolution.

With the above-mentioned input distributions and taking $K = 0.0014\, GeV^2$, we evolve the MD-DGLAP equation and take $F_2 = \sum e_q^2 x(s + v)$ to compare with the HERA (H1

10

and ZEUS) data in Fig. 2. For comparison, we also plot the results of the DGLAP equation with the GRV input (dashed curves). One can see that the contributions of the gluon recombination improve the fit at low Q^2.

3 Unintegrated parton distributions

According to the definition, the two-scale UPDFs and PDFs have the following relations:

$$\int_0^{\mu^2} \frac{dk_t^2}{k_t^2} f_a(x, k_t^2, \mu^2) = xa(x, \mu^2), \tag{14}$$

where $a(x, \mu^2) = v(x, \mu^2)$, $s(x, \mu^2)$ or $g(x, \mu^2)$. Ignoring the fact that the unintegrated density may depend on two scales, one can roughly estimate the unintegrated gluon distribution with

$$\frac{1}{k_t^2} f_g(x, k_t^2, \mu^2 = k_t^2) \simeq \left. \frac{dxg(x, \mu^2)}{d\mu^2} \right|_{\mu^2 = k_t^2}. \tag{15}$$

However, Eq. (15) cannot remain true as x increases, since the negative virtual DGLAP term may exceed the real emission DGLAP contribution and it would give negative values for f_g.

The evolutions of UPDFs on the two scales k_t and μ in the KMR scheme [5] were investigated separately by the real and virtual contributions of Eqs. (1)-(3) , thus we have

$$f_g(x, k_t^2, \mu^2)$$

$$= T_g(k_t^2, \mu^2) \left\{ \frac{\alpha_s(k_t^2)}{2\pi} \int_x^{z_{max}} dz \left[P_{gg}(z) \frac{x}{z} g\left(\frac{x}{z}, k_t^2\right) + P_{gq}(z) \frac{x}{z} V\left(\frac{x}{z}, k_t^2\right) + P_{gq}(z) \frac{x}{z} s\left(\frac{x}{z}, k_t^2\right) \right] \right.$$

$$- \frac{\alpha_s^2(k_t^2) K}{Q^2} \int_x^{1/2} \frac{dy}{y} x P_{gg \to g}(z) \left[\frac{x}{z} g\left(\frac{x}{z}, k_t^2\right) \right]^2$$

$$\left. + \frac{\alpha_s^2(k_t^2) K}{Q^2} \int_{x/2}^x \frac{dy}{y} x P_{gg \to g}(z) \left[\frac{x}{z} g\left(\frac{x}{z}, k_t^2\right) \right]^2 \right\}, \tag{16}$$

$$f_s(x, k_t^2, \mu^2)$$

$$= T_s(k_t, \mu) \left\{ \frac{\alpha_s(k_t^2)}{2\pi} \int_x^{z_{max}} dz \left[P_{qg}(z) \frac{x}{z} g\left(\frac{x}{z}, k_t^2\right) + P_{qq}(z) \frac{x}{z} s\left(\frac{x}{z}, k_t^2\right) \right] \right.$$

$$- \frac{\alpha_s^2(k_t^2)K}{Q^2} \int_x^{1/2} \frac{dy}{y} x P_{gg \to q}(z) \left[\frac{x}{z} g\left(\frac{x}{z}, k_t^2\right) \right]^2$$

$$\left. + \frac{\alpha_s^2(k_t^2)K}{Q^2} \int_{x/2}^x \frac{dy}{y} x P_{gg \to q}(z) \left[\frac{x}{z} g\left(\frac{x}{z}, k_t^2\right) \right]^2 \right\}, \tag{17}$$

$$f_v(x, k_t^2, \mu^2)$$

$$= T_v(k_t, \mu) \frac{\alpha_s(k_t^2)}{2\pi} \int_x^{z_{max}} dz P_{qq}(z) \frac{x}{z} v\left(\frac{x}{z}, k_t^2\right), \tag{18}$$

where $T_a(k_t^2, \mu^2)$ is the Sudakov form factor, resumming the virtual corrections:

$$T_g(k_t^2, \mu^2) = \exp\left\{ -\int_{k_t^2}^{\mu^2} \frac{\alpha_s(k_t'^2)}{2\pi} \frac{dk_t'^2}{k_t'^2} \left[\int_{z_{min}}^{z_{max}} dz \frac{1}{2} P_{gg}(z) + n_f \int_0^1 dz P_{qg}(z) \right] \right\}, \tag{19}$$

$$T_s(k_t^2, \mu^2) = T_v(k_t^2, \mu^2) = \exp\left\{ -\int_{k_t^2}^{\mu^2} \frac{\alpha_s(k_t'^2)}{2\pi} \frac{dk_t'^2}{k_t'^2} \int_0^{z_{max}} dz P_{qq}(z) \right\}. \tag{20}$$

The positive (real) terms on the right-hand sides of Eqs. (1)-(3) describe the number of partons δa emitted in the interval $\mu^2 < k_t^2 < \mu^2 + \delta\mu^2$. Such emission clearly changes the transverse momentum k_t of the evolving parton. While the negative (virtual) contributions in Eqs. (1)-(3) do not change the parton k_t and may be resummed to give the Sudakov form factor $T(k_t^2, \mu^2)$, the parton with transverse momentum k_t remains untouched in the evolution up to the factorization scale.

According to Ref. [16], the strong ordering in transverse momentum automatically ensures angular ordering and the coherence effect constraints

$$z < \frac{\mu}{\mu + k_t} \equiv z_{max}, \qquad (21)$$

and

$$z_{min} = 1 - z_{max}. \qquad (22)$$

On the other hand, there is no coherence effect for quark emission, and therefore the phase

space available for quark emission is not restricted by the angular-ordering condition.

We put the solution of Sec. 2 to Eqs. (16)-(18) and calculate the UPDFs. In Figs.

3-5 we plot x and k_t^2 dependence (solid curves) of the two-scale PDFs in the proton at

the value of the evolution scale $\mu = 10GeV$. For comparison, we give the solutions using

the DGLAP equation with the GRV input (dashed curves). An interesting result is that

the two-scale unintegrated gluon distribution is dropping down for $k_t^2 \to 0$. We indicate

the dip position of the unintegrated gluon distribution by $k_D^2(x)$. In Fig. 6, we plot the

relation $k_D^2(x) \sim x$. We find that k_D^2 is small but it still belongs to the perturbative value

of $k_t^2 > 1 \ GeV^2$ for $x < 10^{-3}$, and this effect can be observed in the RHIC and LHC

energy regions. For comparison, we give the saturation scale $Q_s^2(x) = 1GeV^2(10^{-4}/x)^{0.277}$

[1] in Fig. 6.

Two factors may suppress parton densities at low k_t in the KMR scheme. Factor

A is the valence-like form of the GRV input. For example, we simplify the valence-like

gluon distribution as $xG(x, \mu^2) \sim x^\alpha (1-x)^\beta$ with $\alpha > 0$, and it implies a finite number

of the initial gluons. This distribution is drooping at $x \to 0$. On the other hand, after

evolution begins, the infinite number of the radiative gluons almost have the distribution

$xG(x, Q^2 > \mu^2) \sim x^{\alpha'}(1-x)^{\beta'}$, where $\alpha' \leq 0$. Thus, the distribution fast becomes steep at

small x. This immediate increase of the radiative gluons at small x causes the unintegrated gluon distribution in Eq. (16) to drop down toward small k_t. Factor B is the Sudakov form factor, which is smaller than unity because of the negative contributions of the virtual terms in the DGLAP equation. This factor is irrelative to the parton distributions but becomes small at $k_t^2 \to 0$ if μ^2 is fixed.

To confirm the above suggestion, we look at three different examples:

(i) The drop occurs only from factor A. For this case, we use

$$\frac{1}{k_t^2} f_g(x, k_t^2, \mu^2 = k_t^2) \equiv F(x, k_t^2), \tag{23}$$

to compute the single-scale unintegrated gluon distribution. Note that it is different from Eq. (15), because the contributions of the virtual terms have been removed. The results are plotted in Fig. 7. Comparing Fig. 7 with Fig. 3, we find that the decrease of $F(x, k_t^2)$ delays for $k_t \to 0$, because the Sudakov form factor $T_g = 1$ in Eq. (23).

(ii) The drop occurs from both factors A and B. We see the k_t dependence of the two-scale unintegrated sea quark distribution using the DGLAP equation and the GRV input (dashed curves of Fig. 4(b)). One can find a similar suppression at low k_t as the two-scale unintegrated gluon distribution.

(iii) The drop occurs from factor B, but it is covered by a softer input sea quark distribution. The dropping position $k_D^2(x) \to 0$ in the two-scale unintegrated sea quark distribution using the MD-DGLAP equation (solid curves of Fig. 4(b)) is in this example, where we take a softer sea quark input distribution (see Fig. 1 and Eq. (13)).

We noted that some works [17,18] have used the KMR scheme with the GRV input to calculate exclusive processes. Unfortunately, these works have not presented their

unintegrated gluon distribution in the form $f_g(x, k_t^2, \mu^2)/k_t^2 \sim k_t^2$ as in Fig. 3(b), therefore, the dropping fact in the unintegrated gluon distribution has been hidden.

The μ-dependence of the two-scale unintegrated gluon distribution is plotted in Fig. 8. The results show a quicker dropping for $k_t \to 0$ with increasing μ.

The differences between the solid and dashed curves in Figs. 3 and 4 originate from two sources: one is the direct contributions from the nonlinear terms in the evolution equation; the other is due to the change of the input conditions under shadowing corrections. To illustrate the fist effect, we compare in Figs. 9 and 10 the solutions of the MD-DGLAP equation with and without shadowing corrections using the same input of Eqs. (11) and (13) and $\mu_0^2 = 0.34\,GeV^2$. One can find that the direct nonlinear corrections in the proton are weaker.

We know that the nuclear target is an ideal laboratory for the shadowing research, since the gluon recombination corrections are enhanced as a result of the correlation of gluons belonging to different nucleons at the same impact on a nuclear target. We predict the nuclear parton densities in the MD-DGLAP equation, where the nonlinear terms are multiplied by $A^{1/3}$ [19]. Figures 11 and 12 give the comparisons of the two-scale gluon and sea quark UPDFs at $\mu = 10GeV$ in Pb (A=208) with that in the proton, respectively. In the calculation, the same input, i.e., Eqs. (11) and (13) and $\mu_0^2 = 0.34GeV^2$ are used.[1] Comparing them with Figs. 9 and 10, one can find that the nuclear shadowing effect is important at $x < 10^{-4}$. The geometric scaling implies the following rescaled parton distributions

---

[1]Strictly speaking in the case of a heavy nuclei the input distribution at a low starting scale μ_0 is already modified by the shadowing corrections. However, we have pointed out that these corrections to the integrated parton distributions are small [19]. Therefore, here we have used the *same* input for the *Pb* and for the proton in order to demonstrate the role of gluon recombination in heavy nucleus.

$$f_a(x, k_t^2, \mu^2) = f_a(x/k_t^2, \mu^2). \tag{24}$$

We find that the geometric scaling is not evident in our results, although the x dependence of $f_s(x, k_t^2, \mu^2)$ for the heavy nucleus in Fig. 12 is roughly flat at the small-x limit. It means that the nuclear shadowing behavior is far from the saturation limit.

4 Comparisons with the other parameterizations of UPDFs

Depending on the various QCD evolution dynamics, different unintegrated gluon distributions are proposed. As an example, we make some comparisons of our results with the JS (Jung, Salam) [20,21], KMR (Kimber, Martin, Ryskin) [5], JB (Blümlein) [22] and GBW (Golec-Bier, Wüsthoff) [23] models.

The JS gluon is evolved by using the CCFM equation in a Monte Carlo method. The KMR gluon uses the MRST input distributions and the linear part of Eqs. (16)-(18) but adding the BFKL-ln $1/x$ corrections. The JB gluon assumes that the integrated and unintegrated gluon distributions can be connected by using a universal function, which comes from the expansion of the BFKL anomalous dimension. The comparisons of our (RZ) result with the JS , JB and KMR models are illustrated in Fig. 13, where we use a logarithmic scale to indicate $f_g(x, k_t^2, \mu^2)/k_t^2$. The JS, JB and KMR curves are taken from Ref. [1], in which the flat part of the KMR curve is an assumption but not the evolution result, since the MRST input starts from $\mu_0^2 \simeq 1~GeV^2$. We emphasize that the curves in Fig.13 correspond to the different starting scales and different inputs.

Compared with the JS gluon, the RZ and KMR gluons have a high-k_t tail at small x in Fig. 13, and it can be explained by different factorization schemes. The quark distribution in the RZ and KMR models evolves according to the MD-DGLAP, or DGLAP equations in the collinear factorization scheme. On the other hand, the quark evolution in the JS model with the k_t factorization scheme, is generated by the convolution with off-shell matrix elements for boson-gluon fusion. This additional evolution broadens the k_t spectrum of the quarks. Therefore, the JS gluon needs a narrow k_t spectrum to fit F_2

data. Obviously, these differences arise from different evolution dynamics, and we need more exclusive data to check their predictions.

We find that both the JS and JB gluons tend to rise when $k_t \to 0$ at small x (although the calculation of Ref. [22] shows that the JB gluon suddenly becomes negative at very low $k_t^2 \sim 0.01 \ GeV^2$), whereas the RZ result is asymptotically dropping toward low k_t. As we have emphasized, this behavior is irrelevant to the saturation effect. In fact, saturation is thought to arise from the gluon fusion in some nonlinear evolution equations. The GBW model [23] is one of the models describing saturation using a color-dipole approach. This model parameterizes saturation using the single-scale unintegrated gluon distribution. In Fig. 14 we compare our results (solid curves) obtained using Eq. (23) with the GBW gluon density (dashed curves). One can see that the GBW gluon also vanishes for $k_t \to 0$ due to the nonlinear shadowing effects. On the other hand, the GBW gluon is strongly suppressed for large k_t values, since the parton evolution is not treated in the GBW model.

We noted that a recent work [24] fits low-Q^2 dijet data from the H1 experiment and determines the parameters of the unintegrated gluon density function by using the linear CCFM CASCADE Monte Carlo event generator. It is interesting that compared with their old results, which were determined by fitting F_2 data (dashed curves in Fig. 15), the new parameter (dotted curves in Fig. 15(b)) presents a similar decreasing distribution toward low k_t as our prediction. Note that the curves in Fig. 15 correspond to the different scales and different inputs.

We know that whether a hard valence-like input gluon distribution or a soft one should be taken in the DGLAP evolution is still being argued. Our statement gives a way to test different input models through the observation of the low-k_t behavior of the unintegrated

gluon distribution. Although the application of perturbative QCD at a very lower-k_t region should be done carefully, we find that dropping occurs at low but still perturbative values ($k_D^2 > 1\ GeV^2$ for $x < 10^{-3}$, see Fig.6). We therefore believe that the GRV model provides a possible connection with the nonperturbative region. For example, a vanished unintegrated gluon distribution at $k_t^2 \to 0$ is necessary to obtain a stable $F_L(x, Q^2)$ in k_t factorization [25] and it seems to favor our results with the GRV input.

Since particle production at hadronic collisions is sensitive to the gluon distribution, the various unintegrated gluon distributions are used to explain the particle multiplicities at the RHIC and predict the LHC physics. In this aspect, the search for signatures of gluon saturation effects is a subject of active research. The UPDFs that include a saturation model are used to explain the particle multiplicities at the RHIC, and the results are regarded as an important evidence of saturation effects [17,18,26] In the next section we give a prediction of our (RZ) UPDFs for the inclusive gluon distribution.

5 Prediction of UPDFs for the inclusive gluon distribution

First, we consider the cross section for inclusive gluon production in $proton+proton \rightarrow g$ through the gluonic mechanism $gg \rightarrow g$ at sufficiently high energy [9,17], that is

$$\frac{d\sigma}{dyd^2p_t} = \int I(\varphi)d\varphi, \tag{25}$$

$$I(\varphi) = \frac{4N_c}{N_c^2 - 1}\frac{1}{p_t^2} \int \frac{q_t dq_t}{k_{1t}^2 k_{2t}^2}\alpha_s(\Omega^2)f_{1g}(x_1, k_{1t}^2, p_t^2)f_{2g}(x_2, k_{2t}^2, p_t^2), \tag{26}$$

where $\Omega^2 = \max(k_{1t}^2, k_{2t}^2, p_t^2)$, $k_{1,t}^2 = \frac{1}{4}(p_t^2 + q_t^2 + 2p_t q_t \cos\varphi)$ and $k_{2,t}^2 = \frac{1}{4}(p_t^2 + q_t^2 - 2p_t q_t \cos\varphi)$. The rapidity y of the produced gluon in the center-of-mass frame of pp collision is defined by energy-momentum conservation[27]

$$x_{1/2} = \frac{p_t}{\sqrt{s}}\exp(\pm y). \tag{27}$$

In the computation, an extrapolation of the unintegrated gluon distribution at $k_t^2 \rightarrow 0$ is needed. This region is beyond the perturbative QCD framework. Considering the decreasing behavior of our distribution at $1\ GeV^2 < k_t^2 < k_D^2$ in Fig. 6, we assume

$$f_g(x, k_t^2, p_t^2)/k_t^2 = Ak_t^2, \quad at\ k_t^2 < \mu_0^2, \tag{28}$$

where A is a parameter connecting the two parts of f_g at $k_t^2 > \mu_0^2$ and $k_t^2 < \mu_0^2$.

In Fig. 16, we show the intrinsic angular correlation function $I(\varphi)$ for our model (solid curve) of unintegrated gluon distribution at RHIC energy $W = 200\ GeV$. In this calculation $y = 0$ and $p_t = 1\ GeV$ were taken. A similar correlation function but using

the GBW saturation model is also presented (dotted curve). We also give the result of Ref. [17] (dashed curve), which also uses the KMR scheme with the GRV model, but the flattened distribution of $f_g(x, k_t^2, p_t^2)/k_t^2 = const.$ at $k_t^2 < 0.5 \ GeV^2$ is assumed. One can find that a quite different (oscillatory or flat) pattern is obtained for dropping or not-dropping behaviors of the unintegrated gluon distribution at low k_t. The rapidity distribution is presented in Fig. 17, where the integration over $p_t^2 > 0.34 \ GeV^2$ was performed.

In experiments, a good identification of particles is not always achieved, which makes it hard to determine the rapidity of a particle. The practice then is to measure pseudorapidity. The rapidity and pseudorapidity distributions of partons for massless particles are identical. The situation changes when massive particles are produced in the final state via fragmentation and in this case the rapidity y can be obtained from the pseudorapidity η

$$y = \frac{1}{2} \ln \left[\frac{\sqrt{\frac{m_{eff}^2 + p_t^2}{p_t^2} + \sinh^2 \eta} + \sinh \eta}{\sqrt{\frac{m_{eff}^2 + p_t^2}{p_t^2} + \sinh^2 \eta} - \sinh \eta} \right], \tag{29}$$

where m_{eff} is the mass of the typical produced hadron.[26] Assuming that pions in pp collision are produced via ρ-resonance, we take $m_{eff} = 770 \ MeV$.

To avoid the complicated hadronization dynamics, similar to Ref. [28], we use local parton-hadron duality, that is, the rapidity distribution of particles is identical to the rapidity distribution of gluons. Thus, the pseudorapidity density of the produced charged particles in proton-proton collisions is given by

$$\frac{1}{\sigma_{in}} \frac{d\sigma(\eta, p_t)}{d\eta d^2 p_t} = C J(\eta; p_t; m_{eff}) \left. \frac{d\sigma(y, p_t)}{dy d^2 p_t} \right|_{y=\eta}, \tag{30}$$

where $J(\eta; p_t; m_{eff})$ is jacobian

$$J(\eta; p_t; m_{eff}) = \frac{\cosh \eta}{\sqrt{\frac{m_{eff}^2 + p_t^2}{p_t^2} + \sinh^2 \eta}}, \tag{31}$$

and the gluon to charged hadron ratio via gluon fragmentation model is accounted for by the normalization constant C, which is fixed by the pseudorapidity spectrum of $pp \to \pi^{\pm} X$ at $W = 200 \ MeV$ and $\eta = 0$. Corrections to the kinematics due to the hadron mass are also considered by replacing $p_t^2 \to p_t^2 + m_{eff}^2$ in the evaluation of $x_{1/2}$. Figure 18 gives our prediction, where $C = 0.0153 \ GeV^2$. The experimental data of the UA5 collaboration are taken from Ref. [29]. One can find a sinking platform, which was presented in various saturation models [17,28], but our results are irrelevant to the saturation mechanism.

Our theoretical spectrum in Fig. 18 is too steep to agree with experimental data in the fragmentation region. We noted that the pseudorapidity distribution of charged pions using a saturated unintegrated gluon distribution in the $gg \to g$ mechanism was calculated by Kharzeev and Livin (the KL model) [26] and their results described well the RHIC data. However, contrary to the claim of Ref. [26], a similar calculation was reproduced by Szczurek, who used same KL model in Ref. [17] and his theoretical pseudorapidity distributions are still significantly lower than experimental data in the fragmentation region. This difference originates from the different assumptions used about the unintegrated gluon distribution at the larger x region. In fact, the unintegrated gluon distribution in the KL model is valid with certainty only for $x < 0.1$. To extrapolate the gluon distribution to $x > 0.1$, two different multiple factors $(1 - x)^4$ and $(1 - x)^{5-7}$ in the gluon

distribution are assumed in Refs. [26] and [17], respectively. This uncertainty is now removed, since the UPDFs of our model are well defined in the whole x and k_t space.

It was well known that the recombination of the original fast quarks of two incident hadrons with a slow antiquark cannot be neglected in the fragmentation region [30] Our results in Fig. 16 are compatible with Szczurek's work [17] and they suggest the involvement of other hadronization mechanism in the fragmentation regions. The specificity of this effect will be discussed elsewhere.

Now we use the above results to predict the inclusive pion distribution in the central region ($|\eta| < 2$) at LHC energies. The result for the pseudorapidity density of charged pion in central p-p collisions at $W = 5.5\ TeV$ is shown in Fig. 19. The dashed curves remind us that the quark recombination effects in the fragmentation region are neglected. Comparing the plots with those in Fig. 18, we find that the width of the rapidity distribution increases with increasing energy W. The reason is that the unintegrated gluon distribution is enhanced toward smaller x without saturation behavior in the x distribution in the RZ UPDFs. Thus, either x_1 or x_2 decreases fast with increasing W at a higher fixed value of y, and it leads to broadening of the rapidity distribution with increasing W. It is different from our model in that the x dependence of the unintegrated gluon in the KL model is saturated to a constant at small x and it almost keeps the width of the rapidity distribution, as shown in Ref. [28].

In summary, the unintegrated parton distributions in the proton and heavy nucleus are predicted by using the MD-DGLAP equation incorporating the shadowing corrections, which include exact energy-momentum conservation in each splitting and fusion vertex. We find that the nuclear shadowing effects are obvious although they are far from the

saturation limit. On the other hand, we point out that the suppression of the unintegrated gluon distribution at lower k_t^2 may arise from the valence-like input rather than the saturation effects.

References

[1] B. Andersson et al. (Small x Collaboration), Eur.Phys.J. **C25**, 77 (2002), and references therein.

[2] M. Ciafaloni, Nucl. Phys. **B296**, 49 (1988); S. Catani, F. Fiorani, G. Marchesini, Phys. Lett. **B234**, 339 (1990); S. Catani, F. Fiorani, G. Marchesini, Nucl. Phys. **B336**, 18 (1990); G. Marchesini, Nucl. Phys. **B445**, 49 (1995).

[3] J.Jalilian-Marian, A. Kovner, L. McLerran and H. Weigert, Phys. Rev. **D55**, 5414, (1997); J.Jalilian-Marian, A. Kovner, A. Leonidov and H. Weigert, Nucl. Phys. **B504**, 415 (1997); ibid., Phys. Rev. **D59**, 014014 (1999); H. Weigert, arXiv:hep-ph/0004044; E. Iancu, A. Leonidiv and L. McLerran, Nucl. Phys. **A692**, 583 (2001); ibid., Phys. Lett. **B510**, 133 (2001).

[4] E. Avsar and E. Iancu, arXiv:hep-ph/0901.2873; K. Kutak and H. Jung, arXiv:hep-ph/0812.4082.

[5] M. A. Kimber, A. D. Martin and M. G. Ryskin, Phys. Rev. **D63**, 114027 (2001); M. A. Kimber, A. D. Martin and M. G. Ryskin, Eur. Phys. J. **C12**, 665 (2000).

[6] J. Kwiecinski, A. D. Martin and A. M. Stasto, Phys. Rev. **D56**, 3991 (1997).

[7] I. Balitsky, Nucl. Phys. **B463**, 99 (1996); Yuri V. Kovchegov, Phys. Rev. **D60**, 034008 (1999).

[8] K. Kutak, A.M. Stasto, Eur.Phys. J. **C41**, 343 (2005).

[9] L.V. Gribov, E.M. Levin and M.G. Ryskin, Phys. Rep. **100**, 1 (1983).

[10] A.H. Mueller and J. Qiu, Nucl. Phys. **B268**, 427 (1986).

[11] W. Zhu, Nucl. Phys. **B551**, 245 (1999); W. Zhu and J.H. Ruan, Nucl. Phys. **B559**, 378 (1999); W. Zhu and Z.Q. Shen, HEP & NP, **29**, 109 (2005).

[12] M. Glück, E. Reya and A. Vogt, Z. Phys. **C48**, 471 (1990); ibid., Eur. Phys. J. **C5**, 461 (1998).

[13] J.C. Collins and J.W. Qiu, Phys. Rev. **D39**, 1398 (1989).

[14] W. Zhu, Phys. Lett. **B389**, 374 (1996).

[15] H1 Collaboration, C. Adloff et al., Nucl. Phys. **B497**, 3 (1996); Eur. Phys. J. **C21**, 33 (2001); ZEUS Collaboration, J. Breitweg et al., ibid., **C7**, 609 (1999); Phys. Lett. **B487**, 53 (2000); Eur. Phys. J. **C21**, 443 (2001).

[16] G. Watt, A.D. Martin and M.G. Ryskin, Eur. Phys. J. **C31**, 73 (2003).

[17] A. Szczurek, Acta Phys. Polon. **B34**, 3191 (2003).

[18] M. Luszczak and A. Szczurek, Phys.Rev. **D73**, 054028 (2006); T. Pietrycki and A. Szczurek, Phys. Rev. **D75**, 014023 (2007); R.S. Pasechnik, A. Szczurek and O. V. Teryaev, Phys. Rev. **D78**, 014007 (2008); S.P. Baranov, A.V. Lipatov and N.P. Zotov, Phys. Rev. **D78**, 014025 (2008).

[19] W. Zhu, J.H. Ruan, J.F. Yang and Z.Q. Shen, Phy. Rev. **D68**, 094015 (2003).

[20] H. Jung, G. Salam, Eur. Phys. J. **C19**, 351 (2001).

[21] H. Jung, in Proceedings of the workshop on Monte Carlo Generators for HERA Physics, edited by A. Doyle, G. Grindhammer, G. Ingelman, H. Jung (DESY, Hamburg, 1999), p. 75.

[22] J. Blümlein, DESY Preprint, 95-121, arXiv: hep-ph/9506403.

[23] K. Golec-Biernat, M. Wüsthoff, Phys. Rev. **D60**, 114023 (1999).

[24] A. Knutsson, A. Bacchetta, H. Jung and K. Kutak, arXiv:hep-ph/0808.0847.

[25] J. Blümlein, J. Phys. **G19**, 1623 (1993); B. Badelek, J. Kwiecinski and A. Stasto, Z. Phys. **C74**, 297 (1997); A.V. Kotikov, A.V. Lipatov and N.P. Zotov, Eur. Phys. J. **C27**, 219 (2003).

[26] D. Kharzeev and E. Levin, Phys. Lett. **B523**, 79 (2001).

[27] R.D. Field and R.P. Feynman, Nucl. Phys. **B136**, 1 (1978).

[28] J.L. Albacete, arXiv:hep-ph/0706.1251; Phys. Rev. Lett. **99**, 262301 (2007).

[29] G.J. Alner et al. (UA5 Collaboration), Z. Phys. **C33**, 1 (1986).

[30] K.P. Das and R.C. Hwa, Phys. Lett. **68B**, 459 (1977); R.C. Hwa, Phys. Rev. **D22**, 1593 (1980).

Figure Captions

Fig. 1 Two valence-like input distributions for sea quark: our modified input Eq. (13) (solid curve) and GRV98LO input Eq.(12)(dashed curve). Note that different starting scales μ_0^2 are used.

Fig. 2 The fits of the computed $F_2(x, Q^2)$ in proton by the MD-DGLAP equation (solid curves) comparing with H1 and ZEUS data. The dashed curves are the DGLAP equation results with GRV98LO input.

Fig. 3 The unintegrated, two-scale dependent gluon distribution in proton at $\mu = 10\ GeV$ (a) as a function of x for different values of k_t^2; (b) as a function of k_t for different values of x. The solid (or dashed) curves are the solutions of the MD-DGLAP (or DGLAP) equations, where two different inputs are used. k_D^2 is the dropping scale, where the distribution begins suppression towards lower k_t^2.

Fig. 4 The two-scale unintegrated sea quark distribution in proton at $\mu = 10\ GeV$ (a) as a function of x for different values of k_t^2; (b) as a function of k_t for different values of x. The solid (or dashed) curves are the solutions of the MD-DGLAP (or DGLAP) equations, where two different inputs are used.

Fig. 5 As same as Fig. 4 but for the valence quark distributions.

Fig. 6 The x-dependence of the dropping scale $k_D^2(x)$ for the two-scale unintegrated gluon distribution (solid curve). The dashed curve is the saturation scale according to $Q_s^2(x) = 1\ GeV^2(10^{-4}/x)^{0.277}$.

Fig. 7 Similar to Fig. 3 but for the single-scale unintegrated gluon distribution using Eq. (23).

Fig. 8 The evolution scale μ^2-dependence of the two-scale unintegrated gluon distribution

at $x = 10^{-6}$ for different values of k_t^2.

Fig. 9 Similar to Fig. 3 but using the same input Eqs. (11), (13) and $\mu_0^2 = 0.34 \ GeV^2$.

Fig. 10 Similar to Fig. 4 but using the same input Eqs. (11), (13) and $\mu_0^2 = 0.34 \ GeV^2$.

Fig. 11 Comparison of the two-scale unintegrated gluon distributions in Pb(A=208) (solid curves) with proton (dashed curves) at $\mu = 10 \ GeV$, (a) for x-dependence and (b) for k_t-dependence.

Fig. 12 As same as Fig. 11 but for the two-scale unintegrated sea quark distribution.

Fig. 13 Comparison of our predicted (RZ)-gluon distribution (solid curves) with KMR-gluon (dashed curves), JS-gluon (dotted curves) and JB-gluon (broken-dotted curves), (a) for x-dependence and (b) for k_t-dependence. The dashed and dotted curves are taken from Ref. [1]. Note that the flatten part of the KMR curves is an assumption in Ref. [1] but not the evolution result.

Fig. 14 The single-scale unintegrated gluon distribution using Eq. (23) as a function of k_t^2 for different values of x (solid curves) and the comparison with the saturation GBW model [23] (dashed curves). Note that the GBW gluon lacks a larger k_t tail since the parton evolution is not treated in this model.

Fig. 15 Comparison of our two-scale unintegrated gluon distribution (solid curves) with two results of the CCFM equation in Ref. [24], which are obtained by fitting F_2 data (dashed curves) and low Q^2 di-jet data (dotted curves), respectively.

Fig. 16 The intrinsic azimuthal correlations for different unintegrated gluon distributions: our (RZ) mode (solid curve), GBW model (dotted curve) and Szczurek results [17] (dashed curve).

Fig. 17 Inclusive gluon rapidity distribution ($p_t^2 > 0.34 \ GeV^2$) at $W = 200 \ GeV$ for our

unintegrated gluon distribution.

Fig. 18 Pseudo-rapidity density of charged pion produced in p-p collisions at $W = 200 GeV$. Data are taken from Ref. [29].

Fig. 19 Predicted pseudo-rapidity density of charged pion produced in p-p collisions at $W = 5.5\, TeV$. The dashed curves remind us that the quark recombination effects in the fragmentation region are neglected.
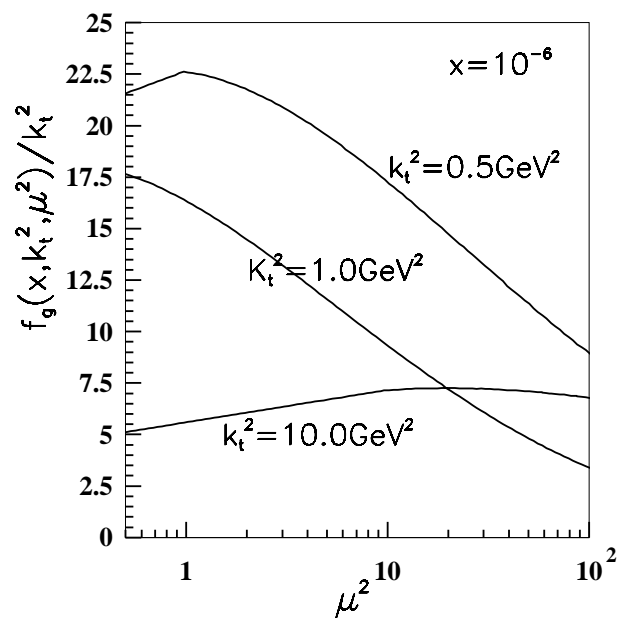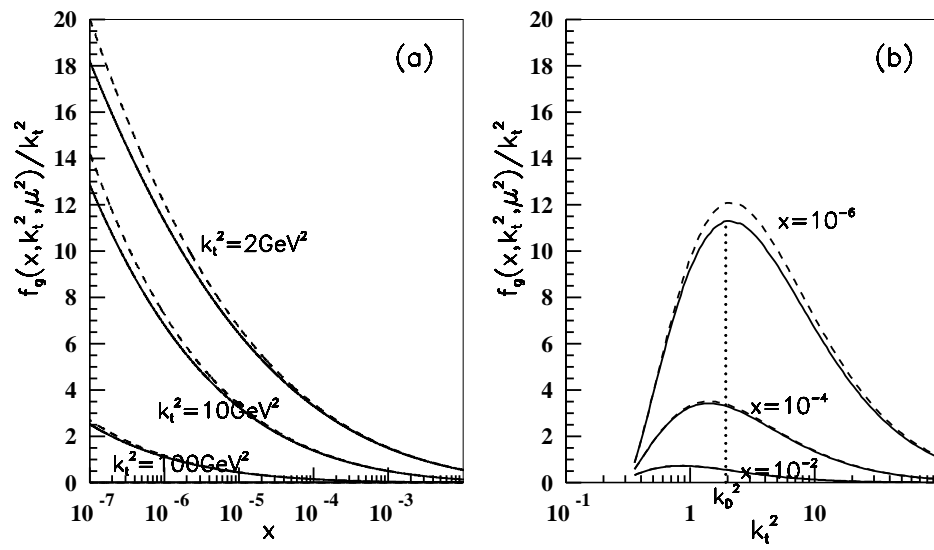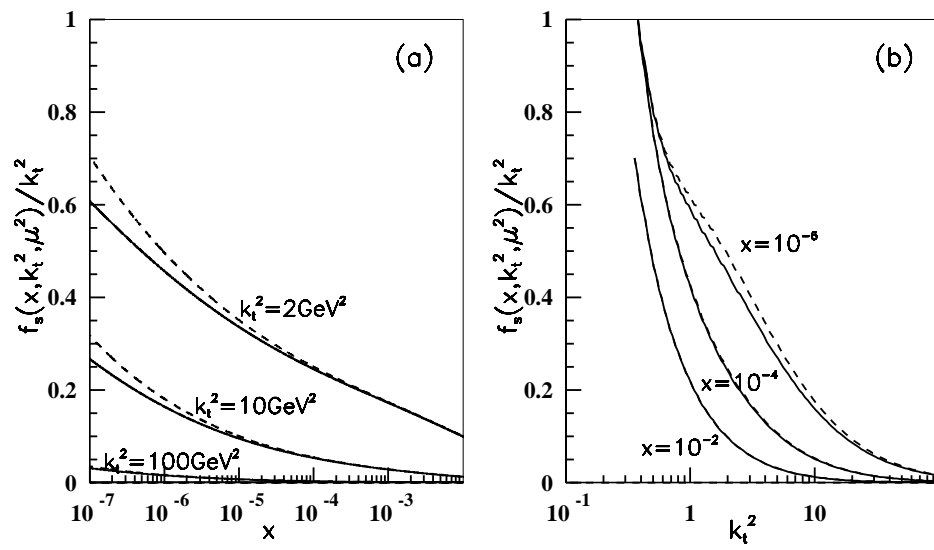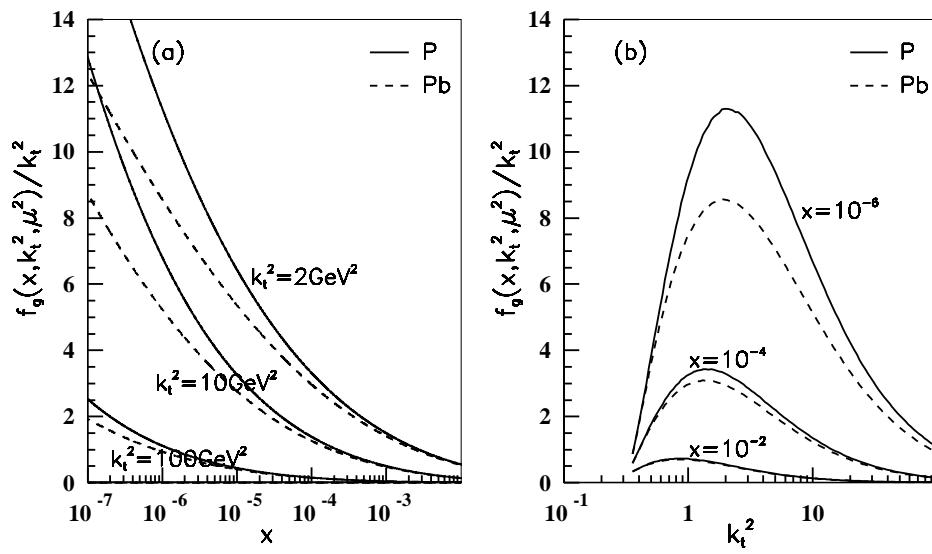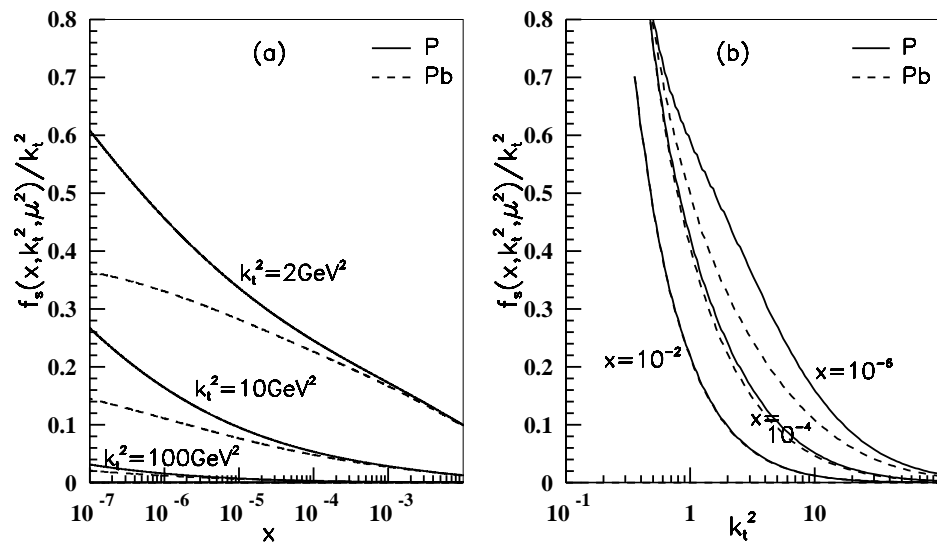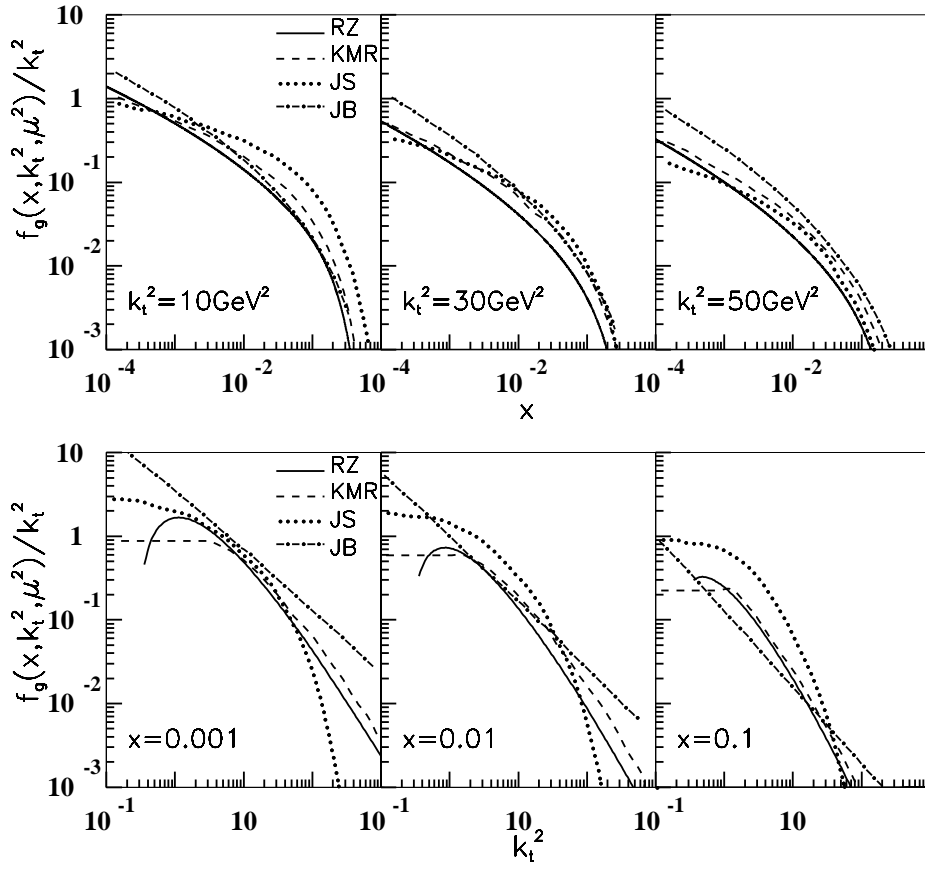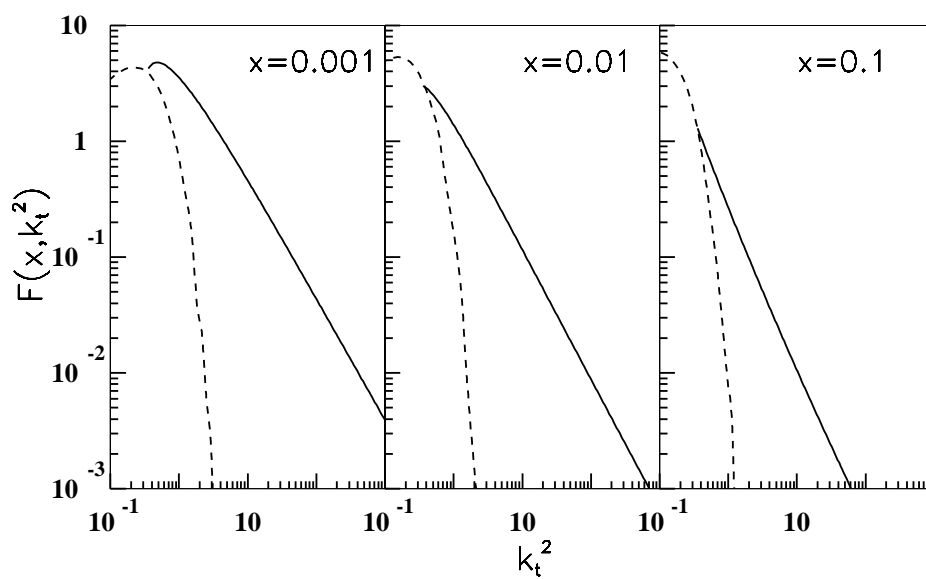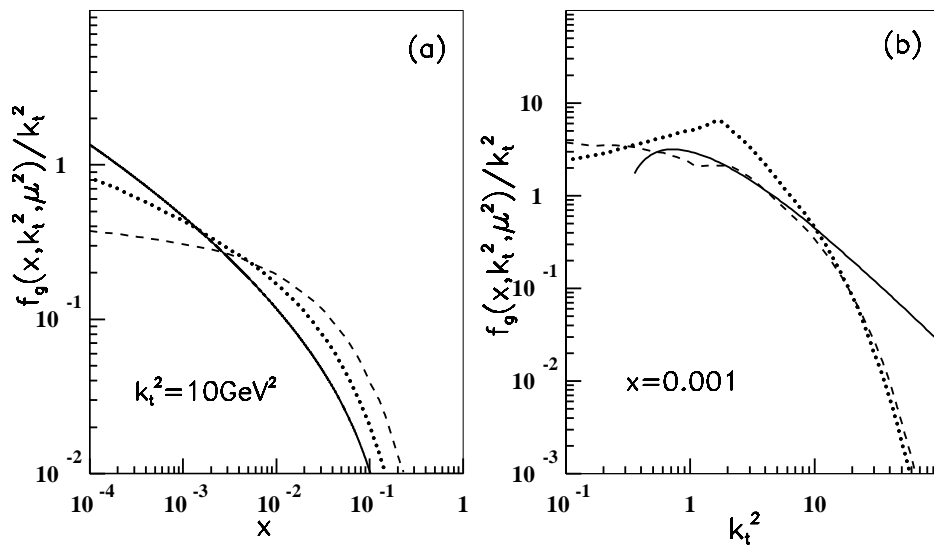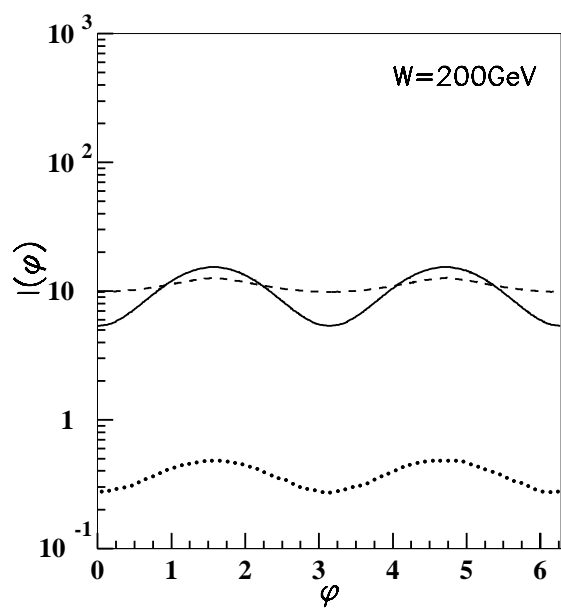
Fig.1

32

Fig.2

33
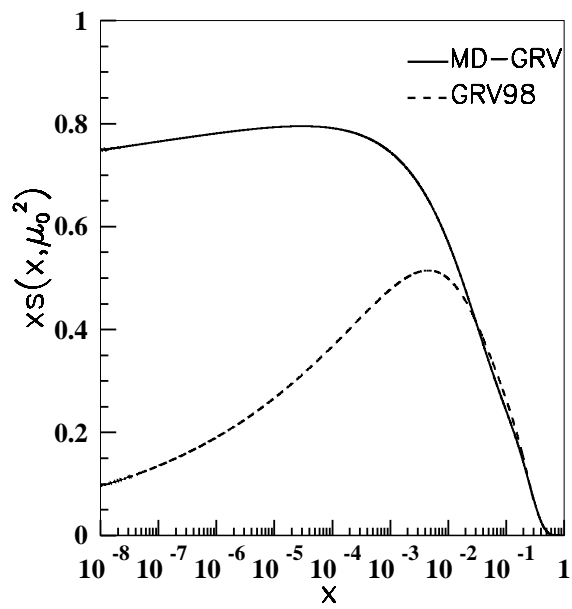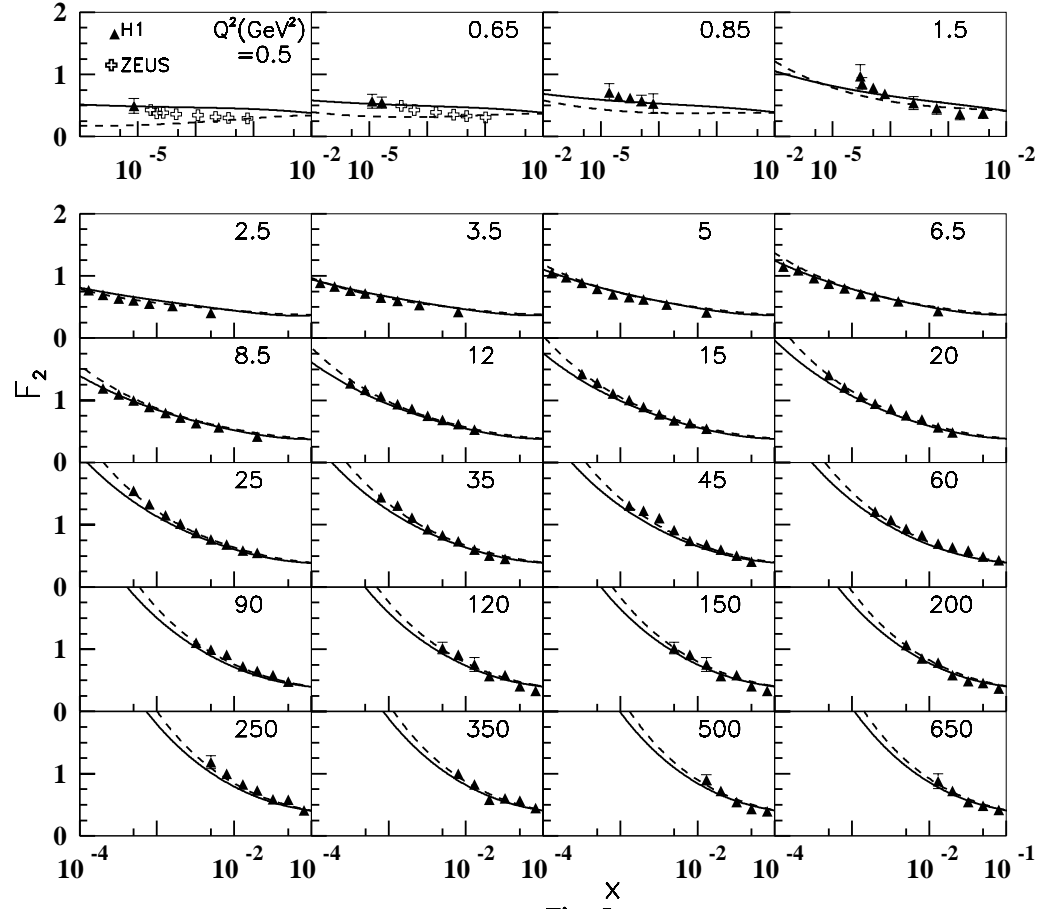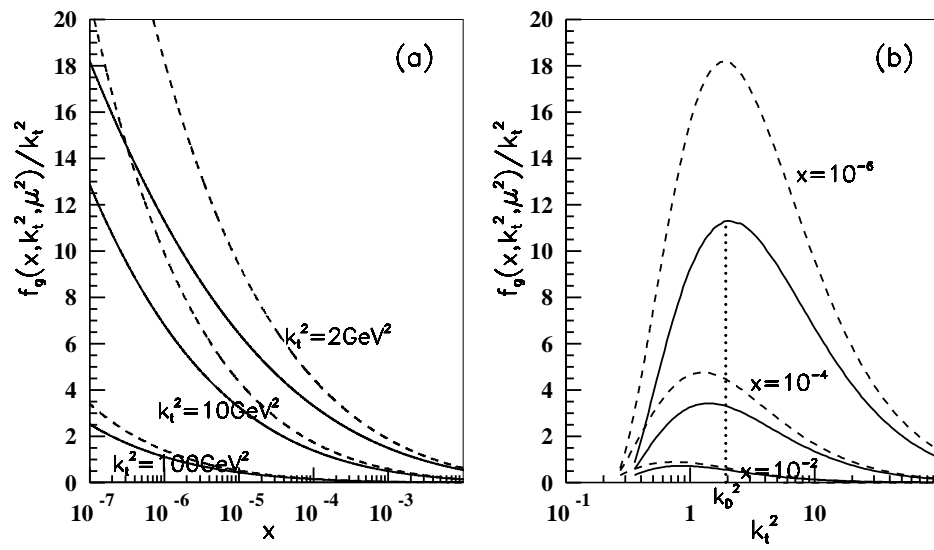
Fig.3
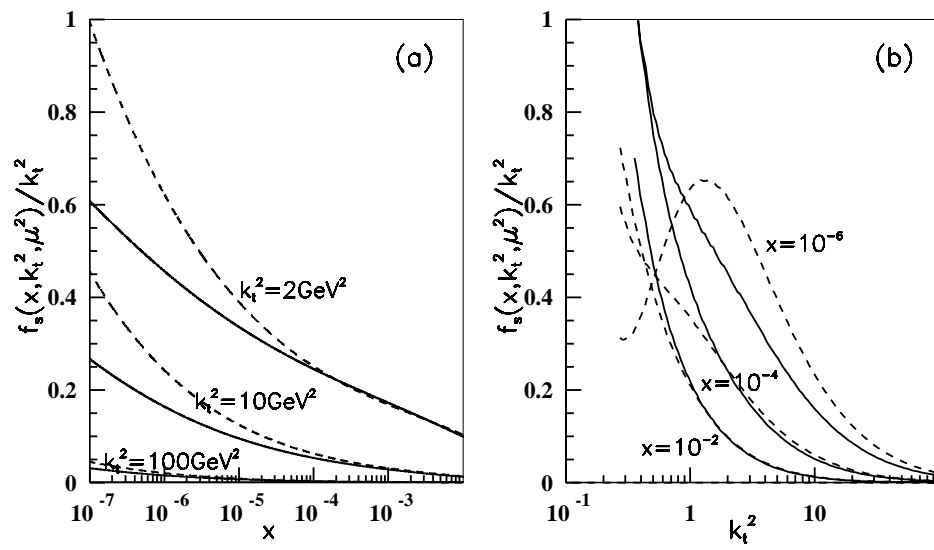
Fig.4
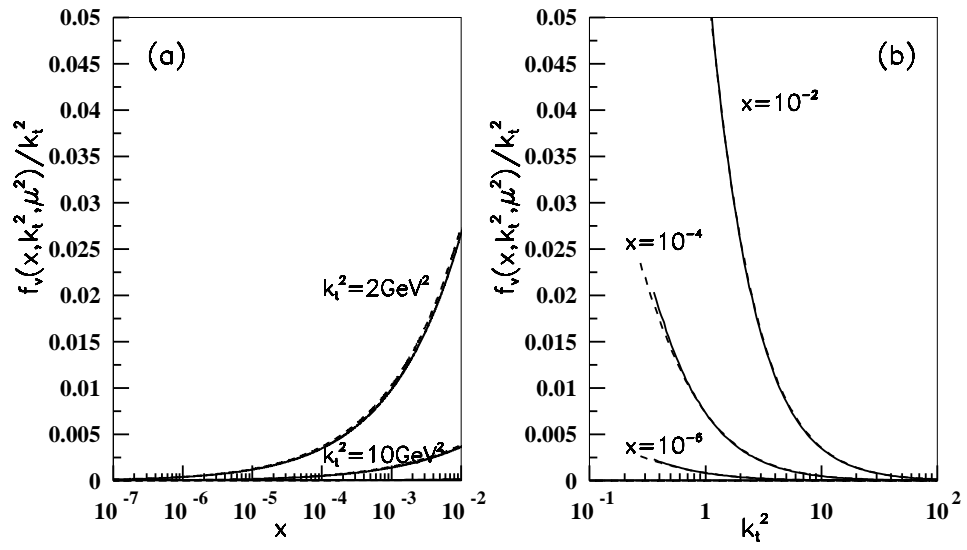
Fig.5
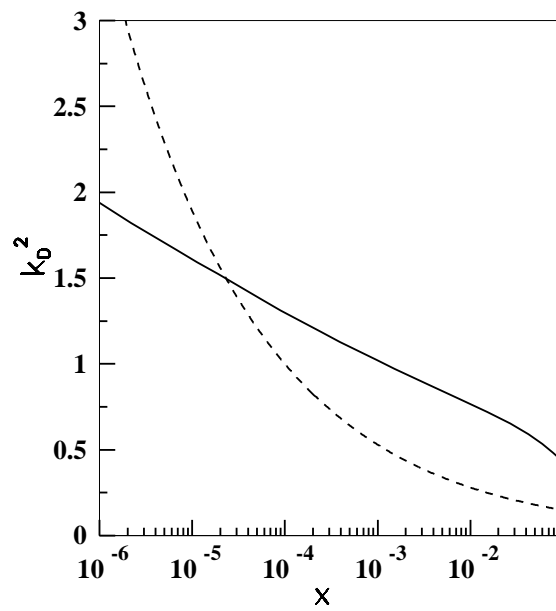
Fig.6
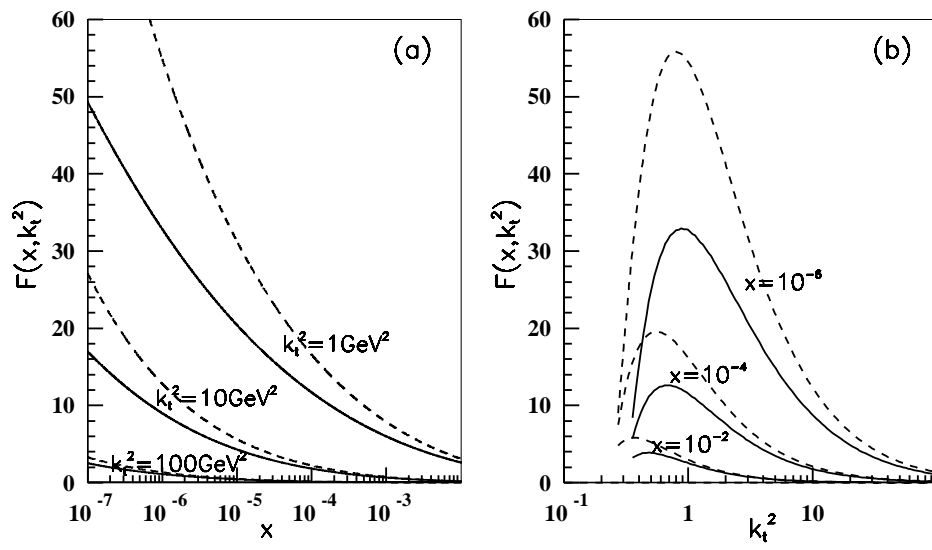
Fig.7

Fig.8

Fig.9

Fig.10

Fig.11

Fig.12

Fig.13

Fig.14

Fig.15

Fig.16

Fig.17

Fig.18

Fig.19